7

Thermoelectric properties of pristine and strained WSSe monolayer

7.1 Introduction

Thermoelectric materials are used for the conversion of waste heat energy into useful electrical energy. In addition, it is also used for thermoelectric cooler without any movable components. The $CoSb_3$ is one of the starting material used for the thermoelectric application, and different modification has been done to improve the performance (D. T. Morelli, T. Caillat, J.-P. Fleurial, A. Borshchevsky, and J. Vandersande, 1995; Heikes, Ure, & Mullin, 1962). The maximum value of the figure of merit (ZT) is approximately 0.52 at 600K for highly doped n-type carriers (Caillat, Borshchevsky, & Fleurial, 1996). Bulk bismuth halides are also widely explored for thermoelectric applications and showed a decent thermoelectric ZT around 0.80 (Kong, 2008; Poudel et al., 2008). The reduction in the size of the particle, the thermoelectric performance improved. Bi_2Te_3 nanomaterials observed the very high ZT around 2.4 compare to bulk material (Hicks, Harman, & Dresselhaus, 1993; L. D. Hicks, 1993). By reducing the thickness of the bulk materials, the thermoelectric performance can be improved, which has also been confirmed theoretically as well as experimentally (Wickramaratne, Zahid, & Lake, 2014a). The power factor of the low dimensional materials enhances due to the increase in the DOS in the valence and conduction bands.

The TMDs based ultrathin 2D materials have been widely studied for thermoelectric applications due to valley dependent electronic properties (Hippalgaonkar et al., 2017). The valley degeneracy improves the power factor, which ultimately enhances ZT of materials. The power factor depends on the electrical conductivity, and Seebeck coefficient. These parameters can be engineered by (i) doping (Kim, Shao, Zhang, & Pipe, 2013), (ii) heterostructure (Lee, Hong, Whangbo, & Shim, 2013), (iii) strain (Bhattacharyya, Pandey, & Singh, 2014), and (iv) electric field effect (Hong, Lee, Park, & Shim, 2016). The heterostructures and valley degeneracy are the two important ways to improve the power factor of TMDs materials (Kumar & Schwingenschlögl, 2015). Janus WSSe monolayer showed the DOS close to WS_2/WSe_2 interface at the valence and conduction band (Chaurasiya, Dixit, & Pandey, 2018b). The biaxial strain can introduce the valley degeneracy at the valence and conduction band edges, leading to enhanced power factor. Lattice thermal conductivity can also be modulated against the biaxial strain, which may assist in improving the overall performance of a thermoelectric device.

7.2 Computational Details

Janus WSSe monolayer is built by replacing the top layer of sulfur of WS_2 by the selenium atom with 25 Å void along c-axis. The WSSe monolayer is relaxed without any constraint. The GGA-PBE (Tasker, 1996) is employed as an exchange-correlation potential throughout the calculation (Giannozzi et al., 2009c). The ultrasoft pseudopotentials are used for the atomic core-shell potential. The energy cutoff for the plane wave is set at 50 Ry. The energy and force cutoff values are 0.0001 Ry and 0.001 Bohr/ $Å^3$, respectively. Monkhorst-Pack scheme is used for

sampling of the BZ. 12x12x1 K-points and BFGS scheme are used for the optimization of the crystal structure. The SCF energy cutoff set at $1x10^{-8}$ Ry. The optimized WSSe monolayer broke the mirror symmetry. The electronic properties are calculated at 24x24x1 K-points, and the tetrahedron method is used for computing the DOS (F. Li, Wei, Zhao, Huang, & Dai, 2017). Boltzmann transport code, based on Boltzmann transport equation, is employed for calculation of thermoelectric properties (Madsen & Singh, 2006). Phonopy and phono3py packages coupled with QE are used for computing the phonon band dispersion and lattice thermal conductivity (Togo, Chaput, & Tanaka, 2015). Phono3py package employs the finite displacement method to calculate the 2nd and 3rd order force constants using a 2x2x1 supercell.

7.3 Results and Discussion

7.3.1Thermoelectric properties of unstrained monolayer

The phonon band dispersion along high symmetry points of BZ are shown in Figure 7.1. The three modes start from zero frequency at the Γ point is acoustic modes, and the rest of the six modes are optical modes. All the vibrational modes have positive or real frequency, which ensures the stability of WSSe monolayer.

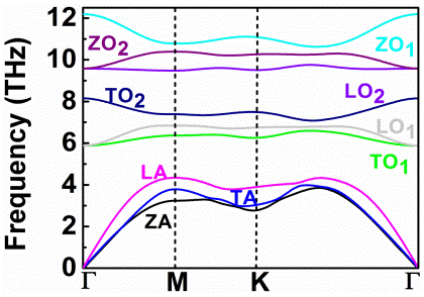

Figure 7.1 Phonon band dispersion curve of Janus WSSe monolayer

Thermoelectric properties are studied in terms of the Seebeck coefficient, electrical conductivity, electronic thermal conductivity, lattice thermal conductivity, power factor and figure of merit. Carrier concentration and density of states play a vital role for thermoelectric properties. The thermoelectric properties with respect to chemical potential are calculated at 300K, 600K, 900K, 1200K and 1500K. The impact of doping density on thermoelectric properties is simulated by changing position of the Fermi level. As the Fermi level shift towards the conduction band ($\mu>0$), negative carrier concentration observed, confirm the n-type doping. However, Fermi level shift towards the valence band ($\mu<0$), ensure the p-type doping with positive carrier concentration shows in Figure 2(a). In the forbidden region there is no carrier density. In addition, the carrier density in valence band and conduction increases with increasing the temperature, shown in Figure 7.2(a). Carrier concentration for n-type carrier is little bit higher than p-type carrier observed. This can be understood from the density of states plot, shown in Figure 2(a). The magnitude of the available states in the conduction band is higher than the valence band. Seebeck coefficient is calculated at different temperatures within the rigid band approximation (RBA) (Bilc, Mahanti, & Kanatzidis, 2006; Chaput, Pécheur, Tobola, & Scherrer, 2005; Das & Soundararajan, 1987). The Seebeck coefficient for $\mu>0$ is negative and $\mu<0$ is positive, ensure the n-type and p-type semiconductor, respectively. The maximum values of the Seebeck coefficient are observed in the forbidden region and its decline with towards the valence band because it has the inverse relation with the carrier concentration. The Seebeck coefficient is highly sensitive to temperature and it decreased with increasing the temperature. Seebeck coefficient value for p(n) type carrier are 2756 (-2750), 1360 (-1375), 886 (-908), 653 (-682) and 521 (-552) μV/K at 300K, 600K, 900K, 1200K and 1500K, respectively. At 300K, Seebeck coefficient is higher for p-type carriers

and at higher temperature (Above 300K) the Seebeck coefficient for n-type carrier is dominated. The computed Seebeck coefficient values are comparable with the bulk WS_2 (Gandi & Schwingenschlögl, 2014). The optimal value of Seebeck coefficient is relatively large for n-type carriers as compared to p-type carriers, and thus, maybe an indication towards the contribution of n-type carriers in improving thermoelectric performance. The Seebeck coefficient usually depends on the density of states and effective mass at the valence and conduction band edge. The DOS near band edges can be improved by increasing the number of valleys and the higher effective mass can be achieved because of flatness of the bands near edges. Strain is used as an external stimulus to tailor the valley near band edges, and thus, the thermoelectric properties of the material can be improved.

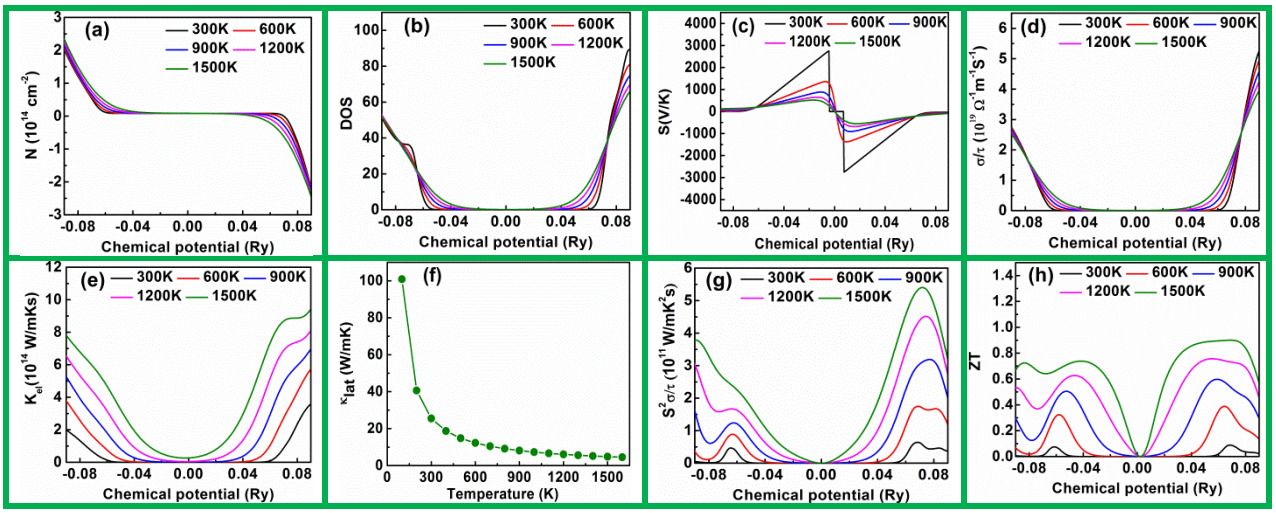

Figure 7.2(a) Carrier concentration, (b) density of states, (c) Seebeck coefficient, (d) electrical conductivity, (e) electronic thermal conductivity, (f) lattice thermal conductivity, (g) power factor and (h) figure of merit versus chemical potential of unstrained WSSe monolayer.

Electrical conductivity (σ/τ) at different temperature is shown in Figure 7.2(d). Electrical conductivity is almost zero and it's increasing with increasing the chemical potentials towards the valence band and conduction band. Electrical conductivity is increasing with increase in temperature. It's proportional to the carrier concentration and also increases with temperature. Electrical conductivity is higher for n-type carrier than p-type carrier. The reason is because carrier concentration is higher for n-type carrier than p-type carrier. We find that the electrical conductivity increases with increasing the carrier concentration; however, it is relatively less sensitive to temperature as compared to Seebeck coefficient. The electrical conductivity is in the order of $10^{19}\Omega^{-1}m^{-1}S^{-1}$. The computed ratio of electronic thermal conductivity to the scattering time is shown in Figure 7.4 for n and p-type carriers. We noticed that electronic thermal conductivity is also showing a similar trend, like electronic conductivity. Further, the electronic thermal conductivity is more sensitive to the temperature. At room temperature, electronic thermal conductivity is almost zero in the forbidden region and further increasing the temperature forbidden region reduced and electronic thermal conductivity improved. The electronic thermal conductivity is higher for n-type carrier than the p-type carrier. The values of electronic thermal conductivity for p-type carrier are $1.98x10^{14}$, $3.76x10^{14}$, $5.25x10^{14}$, $6.25x10^{14}$ and $7.8x10^{14}$ W/mKs for 300K, 600K, 900K, 1200K and 1500K, respectively. In addition, the thermal conductivity for n-type carrier is $3.59x10^{14}$, $5.74x10^{14}$, $6.98x10^{14}$, $8.12x10^{14}$ and $9.49x10^{14}$ W/mKs for 300K, 600K, 900K, 1200K and 1500K, respectively. This value is lower than that for other TMDs such as bulk WS_2 where the maximum value reaches nearly $1x10^{16}$ $Wm^{-1}K^{-1}s^{-1}$, suggesting that WSSe monolayer may exhibit better thermoelectric performance with the optimal electronic contribution to the thermal conductivity. Further, this value is comparable to that of $MoSe_2$ and WSe_2 monolayers,

showing electronic thermal conductivity in the range $1.5x10^{15}$ -$1.8x10^{15}$ $Wm^{-1}K^{-1}s^{-1}$ and $1.5x10^{15}$ - $2.2x10^{15}$ $Wm^{-1}K^{-1}s^{-1}$, respectively.

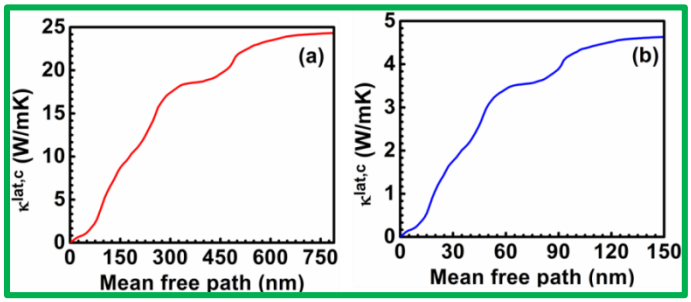

Figure 7.3 Cumulative thermal conductivity versus mean free path of WSSe monolayer at (a) 300K and (b) 1500K

The temperature dependent lattice thermal conductivity is shown in Figure 7.2(f), suggesting that it is decreasing with an increase in temperature because phonon scattering dominates over phonon interaction at high temperature. Bose-Einstein distribution gives the relation of phonon distribution at a specific temperature (Dove, 1993). The temperature gradient causes the phonon diffusion from hot to a cold region, resulting in heat flow. These phonons will pass through the material, and scattering will take place, altering the phonon direction under Umklapp scattering. According to BTE, the rate of change of phonon distribution vanishes in the steady state (Grund & Erscheinungen, 1914). That's why we used linear BTE (Ziman & Levy, 2001), where derivative of the phonon distribution with respect to temperature is replaced with equilibrium Bose-Einstein distribution derivative (Omini & Sparavigna, 1995). The phonons are mainly scattered by other phonons i.e., phonon-phonon scattering is dominant in a single crystal. The scattering time for one phonon depends on others due to the three phonon phenomenon in scattering events (Kundu, Mingo, Broido, & Stewart, 2011). Thermal conductivity depends on phonon lifetime, frequencies, group velocity, and distribution function (Subhash L. Shindé, 2014) and is an integral over a BZ. The computed lattice thermal conductivity for Janus WSSe monolayer is lower than that of WSe_2 and $MoSe_2$ bulk and monolayers. In contrast to single crystal, a polycrystalline material consists of randomly oriented small crystallites, separated from each other by finite boundaries. These crystallites are known as grains, and the boundaries are known as grain boundaries. Since, the atomic arrangement in one grain is different from other grain, and thus, a phonon approaching the grain boundaries will experience scattering at such grain interfaces (Ziman & Levy, 2001). Nanostructures are prone to defects, which may exhibit such scattering in contrast to the phonon-phonon scattering, which dominates in single crystal or in materials where the grain sizes are usually greater than the phonon mean free path (mfp). The computed cumulative thermal conductivity, $\kappa^{lat,c}$ (CTC) is plotted in Figure 7.3(a & b) as a function of mfp at 300 K and 1500 K. We noticed that with lower mfp, CTC values reduces substantially, Figure 7.3, suggesting that the thermal conductivity will decrease in case of grain boundary scattering. The CTC as a function of mfp is a useful parameter to understand the requirement of nanostructuring for reducing κ_{lat}, which is sum κ_{lat} due to the phonons having mfp less than or equal to that particular mfp. Further, κ_{lat} at higher temperature i.e., 1500 K, is lower than that of at 300 K, shown in Figure 7.3. This can be attributed to the contribution from both phonon-phonon and grain boundary scattering at higher temperatures, reducing the overall thermal conductivity. The κ_{lat} can be reduced up to 50% or more by reducing the flake size of monolayer to about 225 nm and 41 nm at 300 K and 1500 K, respectively, Figure 7.3. The contribution of electron-phonon and electron-impurity scattering to the relaxation time τ, and their relative strength are important to understand. The relaxation time-dependent electrical conductivity and electronic contribution to the lattice thermal conductivity help to predict the figure of merit. We computed relaxation time using the equation $\tau = (\mu^*m)/e$, where μ is mobility, m is effective mass, and e is electronic charge

for WSe_2 monolayer (Aivazian et al., 2015; Allain & Kis, 2014; Schmidt, Giustiniano, & Eda, 2015b). The computed relaxation time is $1.63x10^{-13}$ s. The computed relaxation times are comparable to the earlier reported relaxation times (Kumar & Schwingenschlögl, 2015).

To obtain the high value of figure of merit, the power factor should be high. The thermoelectric power factor relies on Seebeck coefficient and electrical conductivity, which are calculated for unstrained WSSe monolayer and used to compute the power factor, Figure 7.2(g). Room temperature thermoelectric power factor (relaxation time scaled) for p-type carriers is $0.46x10^{11}$ W/mK^2s and further increase the temperature the power factor improved 0.89, 1.57, 3.05 and 3.79 W/mK^2s at 600K, 900K, 1200K and 1500K, respectively. Moreover, the power factor for n-type carriers is 0.64, 1.75, 3.19, 4.51 and 5.40 W/mK^2s at 300K, 600K, 900K, 1200K and 1500K, respectively. The thermoelectric power factor is around 50% higher for n-type carriers compare to p-type carriers, which ensure that n-type doping is more preferable for WSSe monolayer. The two different peaks correspond to the n-type carriers at lower temperature at or below 600K and further increasing the temperature its merge into the one peak, which can be understood from the DOS diagram. Figure 7.2(h) shows the computed figure of merit against chemical potential at 300 K, 600 K, 900 K, 1200 K, and 1500 K. The maximum ZT values are 0.74 and 0.90 at 1500K for p-type and n-type carrier carriers, respectively. These values are comparable or more than that of bulk and monolayer other TMDs like MoS_2, $MoSe_2$, WS_2 and WSe_2 (Bera & Sahu, 2019; Dimple, Jena, & De Sarkar, 2017; Gandi & Schwingenschlögl, 2016; Huang, Da, & Liang, 2013; Huang, Luo, Gan, Quek, & Liang, 2014; Z. Jin et al., 2015; queksy, 2012; Tani & Kido, 2007; Wickramaratne, Zahid, & Lake, 2014b; Xiang et al., 2019; L. D. Zhao et al., 2016). This is because of the intermediate electronic, lattice, and optical properties of Janus WSSe monolayer with respect to the parent WS_2 and WSe_2 monolayers. The maximum value of ZT for bulk WSe_2 is 0.81 and 0.65 at 1200 K for n-type and p-type charge carriers, respectively (Kumar & Schwingenschlögl, 2015). The computed ZT values for Janus WSSe monolayer are 0.76 and 0.63 at 1200 K for n-type and p-type charge carriers, respectively. The obtained ZT for p-type carriers is comparable with both bulk and monolayer of WSe_2, whereas ZT value is little bit lower than that of WSe_2 monolayer for n-type charge carriers(Kumar & Schwingenschlögl, 2015). These values i.e., ZT for bulk WS_2 are 0.7 and 0.4 at 1500 K for n-type and p-type charge carriers, respectively (Gandi & Schwingenschlögl, 2014). These thermoelectric parameters are similar to that of other TMD systems, and thus, WSSe monolayer can also exhibit good thermoelectric characteristics for p-type carriers.

7.3.2Thermoelectric properties of biaxial strained monolayer

The external strain is one of the effective way to enhance the thermoelectric properties of materials (Bhattacharyya et al., 2014; D. Guo, Hu, Xi, & Zhang, 2013; Lv, Lu, Shao, Lu, & Sun, 2016; Lv, Lu, Shao, & Sun, 2014). It can tailor the band gap and valley degeneracy at the edge of conduction and valence band edge, which may improve the Seebeck coefficient and electrical conductivity. The valleys are considered degenerate when there is no or very small energy difference (< 26 meV) in valley energies with respect to the band extreme for a number of bands. We investigated the dynamic stability of WSSe monolayer against strain, and the computed phonon dispersion curves are plotted for different strain values, ranging from -6% to 8% with an interval of 2%, Figure 7.4. The strain also leads to the softening of acoustic and optical phonon modes and thus, lowering the lattice thermal conductivity. The acoustic modes showed small deviations at Γ point with very small imaginary frequency suggests dynamic stability of the monolayer against strain. The phonon band dispersions ensure the dynamic stability of WSSe monolayer from 6% compressive strain to 8% tensile strain.

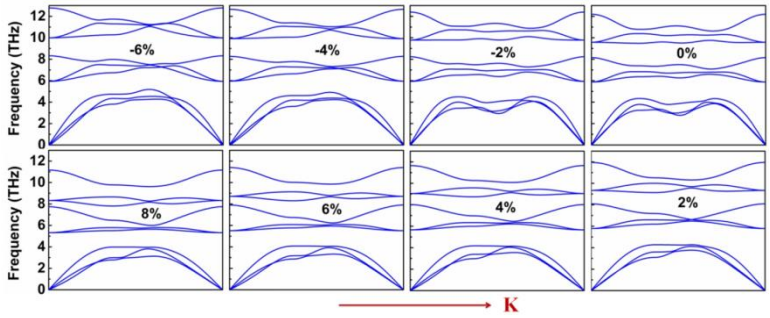

Figure 7.4 Comparison of phonon band softening and/or hardening under the compressive and tensile strains. Here K refers Γ-M-K-Γ direction.

The strain engineering leads to the change in electrical properties of the materials due to the presence of light and heavy bands at the edge of the valence and conduction bands (Zou, Xie, Liu, Lin, & Li, 2013). The band gap variation under the biaxial tensile and compressive strains is reported in our recent report (Chaurasiya et al., 2018b). There are studies on many transition metal dichalcogenides materials, showing strain induced valley degeneracy or band convergence (Dimple et al., 2017). We showed the variation in valence, and conduction bands under biaxial tensile and compressive strains in Figure 7.5. Further, valley degeneracy is also noticed in the Janus WSSe monolayer under the biaxial tensile and compressive strains. The strain induced valley degeneracy also leads to the change in electrical conductivity, Seebeck coefficient, and thermal power factor because of the change in different atomic orbital characteristics under strain. In addition to strain, the valley degeneracy can also be realized by modulating the layer thickness, and external electric field (Hong et al., 2016). The onset of valley degeneracy is shown in Figure 7.5 at the edge of the VBM and CBM under the tensile and compressive strains. The valley degeneracy modulated electrical conductivity and Seebeck coefficient for two valleys degeneracy at the VBM or CBM are expressed as a weighted factor as

$$\text{Electrical conductivity } (\sigma) = \sigma_1 + \sigma_2$$

$$\text{Seebeck coefficient (S)} = \frac{S_1\sigma_1 + S_2\sigma_2}{\sigma_1 + \sigma_2}$$

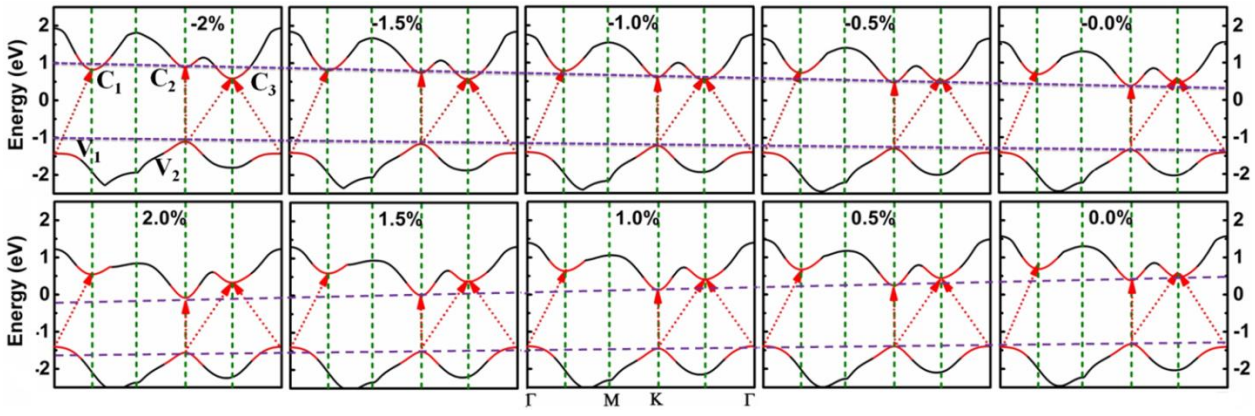

Figure 7.5 Variation of the valence and conduction band edges under the biaxial compressive and tensile strains

The electronic band structure shows three valleys in the conduction band, which are C_1 at mid of Γ-M, C_2 at K, and C_3 at mid of Γ-K points, shown in Figure 5. Moreover, the valence band also exhibits two valleys: V_1 at Γ and V_2 at K point. These valleys are shifted upward or downward according to applied strain and modify the electrical conductivity and Seebeck coefficient accordingly. In unstrained monolayer, conduction band valleys C_2 and C_3 have an energy

difference of 70 meV. However, the valence band valleys V_1 and V_2 show 100 meV energy difference. At high temperature above 900 K, thermal energy is sufficient, so conduction band valleys C_2 and C_3 contribute to the electrical conductivity and Seebeck coefficient. The valleys C_2 and C_1 are shifted upward away from Fermi level due to the compressive strain, but the rate of shifting valley C_2 is more with respect to valley C_1. However, the valley C_3 is not showing any shift with the compressive strain. At 0.5% compressive strain, valleys C_2 and C_3 become degenerate and contribute in improving the n-type electrical conductivity and Seebeck coefficient. Further, increasing the compressive strain, i.e. at 1.5%, valleys C_1, and C_2 become degenerate, and thus, again improves the n-type electrical conductivity and Seebeck coefficient. Initially, in unstrained monolayer, the valence band valleys V_1 and V_2 contribute significantly to the p-type electrical conductivity and Seebeck coefficient. Moreover, further increasing the compressive strain, valley V_1 is not shifting while valley V_2 is shifted upward. The energy difference between V_1 and V_2 is continuously increasing with the compressive strain, which leads to a reduction in the p-type electrical conductivity and Seebeck coefficient. The difference in energy between the valleys of the conduction band and conduction band up to 100 meV can contribute to thermoelectric properties. This valley degeneracy also results in enhanced thermoelectric properties for n-type and p-type carrier concentrations. The conduction band valleys C_1, C_2, and C_3 shifted towards the Fermi level on applying tensile strains, but the rate of shifting of valley C_2 is higher with respect to valley C_1, and valley C_3. The energy difference between these conduction band valleys is continuously increasing with a tensile strain resulting in a decrease in the thermal transport for n-type carriers. However, the valence band valley V_1 is not shifting and V_2 is shifting away from the Fermi level under tensile strain. At 1% tensile strain, the valleys V_1 and V_2 become degenerate, and both contribute to the p-type electrical conductivity and Seebeck coefficient. Further increasing the tensile strain, the energy difference between V_1 and V_2 has increased, making them non-degenerate. The valley degeneracy in the conduction band improves the n-type thermoelectric properties, while valley degeneracy in the valence band improves the p-type thermoelectric properties.

The Seebeck coefficient, with n and p-type carriers are computed at different biaxial tensile and compressive strains for 300K, 600K, 900K, 1200K, and 1500K, and summarized in Figure 7.6. The Seebeck coefficient decreases with increasing the carrier concentration, can be understand using the equation given below (Ibrahim M Abdel-Motaleb, 2017)

$$S = \frac{8\pi T k_B^2}{3eh^2} m^* \left(\frac{\pi}{3n}\right)^{2/3}$$

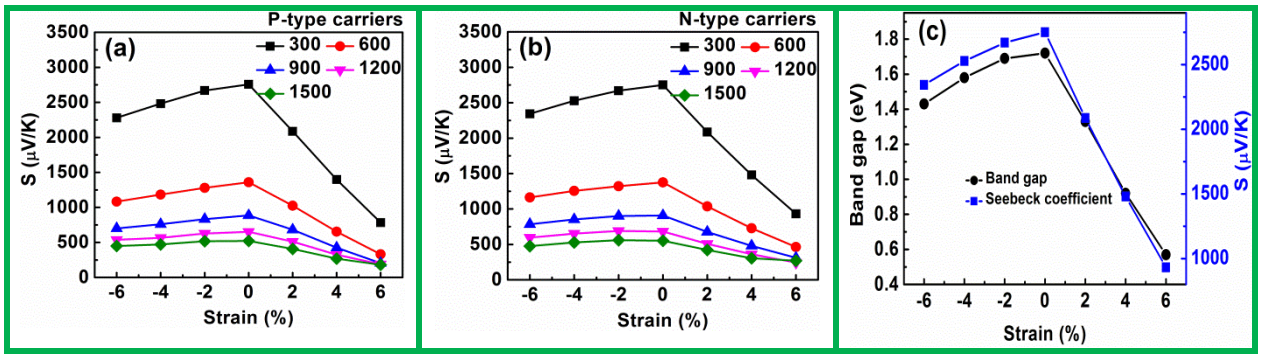

Figure 7.6 Strain dependent Seebeck coefficients for (a) p-type carriers, (b) n-type carriers and (c) band gap and Seebeck coefficient.

Where T, k_B, e, m^* and h are the temperature, Boltzmann's constant, electronic charge, effective mass, and Plank constant, respectively. The carriers close to the VBM and CBM play an important role in the conduction process at the finite temperatures. Fermi level shifts near to the band edge because of carrier doping, and thus, large numbers of energy states will be available for

conduction on both sides, which should result in tailor Seebeck coefficient and electrical conductivity. The strain changes the electronic band gap, which changes the carrier's effective mass. Seebeck coefficient is proportional to the effective mass of the carrier. The results showed the valley degeneracy for unstrained i.e., pristine WSSe and thus, suggesting the maximum Seebeck coefficient value for both n and p-type carriers, which decreases for both compressive and tensile strains. For n-type carriers, Seebeck coefficient value for unstrained monolayer is about 17% and 34% more at 6% compressive and 6% tensile strains, respectively, at 1500 K temperature. The value of Seebeck coefficient for unstrained monolayer is about 21% and 40% more than Seebeck coefficient at 6% compressive and 6% tensile strains, respectively, for similar p-type carriers and at 1500K. The high Seebeck coefficient value is attributed to the high density of states and effective mass $m_d^* = N_v^{2/3} m^*$ (Alsaleh, Shoko, & Schwingenschlögl, 2019). $N_v$refers to the number of degenerate valleys. The higher N_v will enhance m_d^*, which finally will increase the Seebeck coefficient. Further, we plotted strain dependent Seebeck coefficient for biaxial strains in Figure 6. Note that here, highest value of Seebeck coefficient is plotted for n and p-type carriers. We also notice that the Seebeck coefficient is decreasing with increasing temperature for both tensile and compressive strains, suggesting the semiconductor behavior. The variation in Seebeck coefficient under strain exhibits similar trends like band gap, which can be validated using Goldsmid-Sharp relation $E_g = 2\, e\, S_{max} T_{max}$ (Goldsmid & Sharp, 1999), where E_g stands for band gap, S_{max} is the maximum value of Seebeck coefficient at T_{max}. This is summarized in Figure 7.6(c), showing Seebeck coefficient and band gap against strain, and a one to one correspondence between these quantities can be observed.

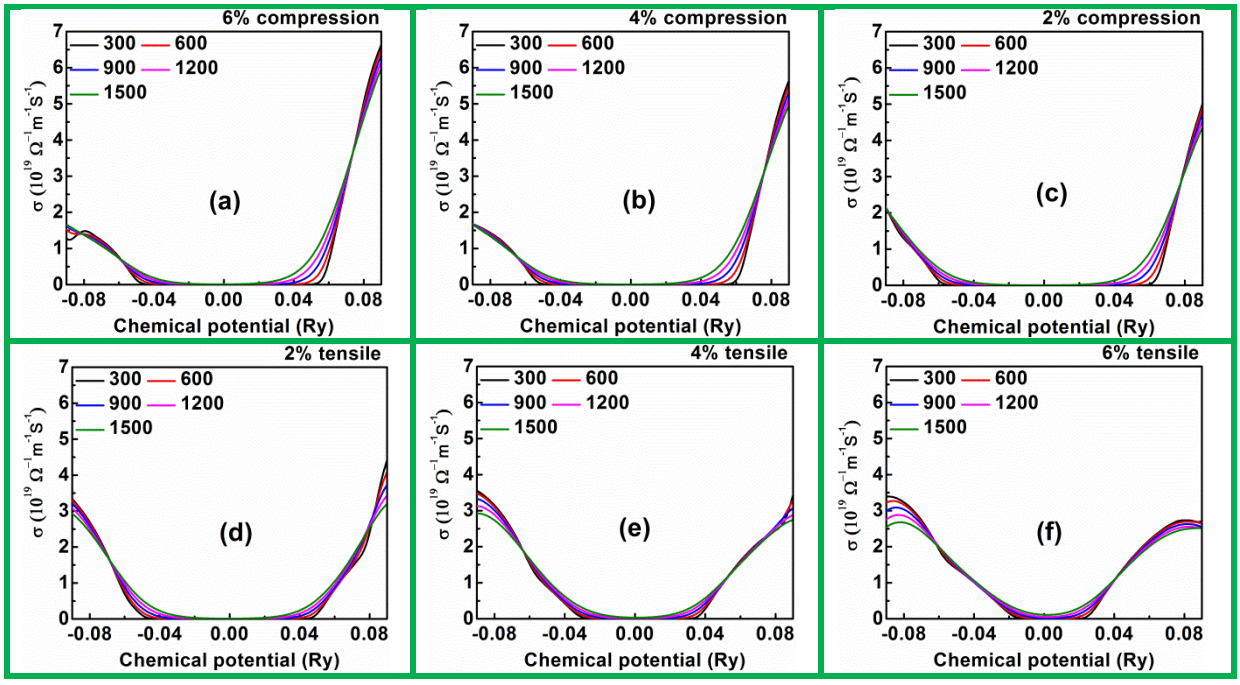

Figure 7.7 Chemical potentials dependent electrical conductivity of WSSe monolayer at different temperatures for (a) – 6%, (b) - 4%, (c) -2%, (d) 2%, (e) 4% and (f) 6% strain (negative sign indicates the compressive strain and postitive sign indicates the tensile strain)

The electrical conductivity plot with respect to the chemical potentials for different temperatures together with biaxial tensile and compressive strains is shown in Figure 7.7. We find that the electrical conductivity is increasing with increasing the chemical potential (carrier concentration) and is less sensitive to temperature, unlike the Seebeck coefficient. Further, the light bands in the electronic band structure provide good electrical conductivity, which is more sensitive to the band gap of the material. The band gap of the Janus WSSe monolayer decreases under the compressive strain. In addition, the band gap also decreases with increasing the tensile strain.

The electrical conductivity under the compressive and tensile strains is calculated for n-type and p-type carriers at different temperatures are shown in Figure 7.7. Additionally, electrical conductivity can be improved more effectively under tensile strain because of larger band gap reduction under tensile strain. The electrical conductivity also depends on the mobility of the charge carrier, which relies on the effective mass and relaxation time. The effective mass will depend on the band convergence at the band edge, which is responsible for electrical conduction, and the relaxation time depends on the temperature as well. The relaxation time is the power function of the carrier energy, temperature and effective mass as $\tau \propto E^{\Gamma} T^{S} (m^{*})^{t}$; where E is the energy of the electron (Shuai et al., 2017). Further, the mobility can be improved by tuning the effective mass together with band gap and reducing the carrier scattering, which ultimately improves the electrical conductivity. The electrical conductivity increased with increasing the temperature at low carrier concentration, whereas, at the higher carrier concentration, the electrical conductivity is insensitive to the temperature.

Chemical potential dependent electronic thermal conductivity at different temperature for tensile and compressive strain is shown in Figure 7.8. The electronic thermal conductivity is increasing with increasing the compressive strain for n-type carriers. For n-type carriers, the electronic thermal conductivity at 1500K is 17.7x10^{14}, 14.4x10^{14} and 12.2x10^{14} W/mKs for 6%, 4% and 2% compressive strain. In addition, the tensile strain also enhanced the electronic thermal conductivity for n-type carriers. The electronic thermal coductivity for 2%, 4% and 6% tensile strain is 7.81x10^{14}, 8.4x10^{14} and 9.9x10^{14} W/mKs, respectively at 1500K.

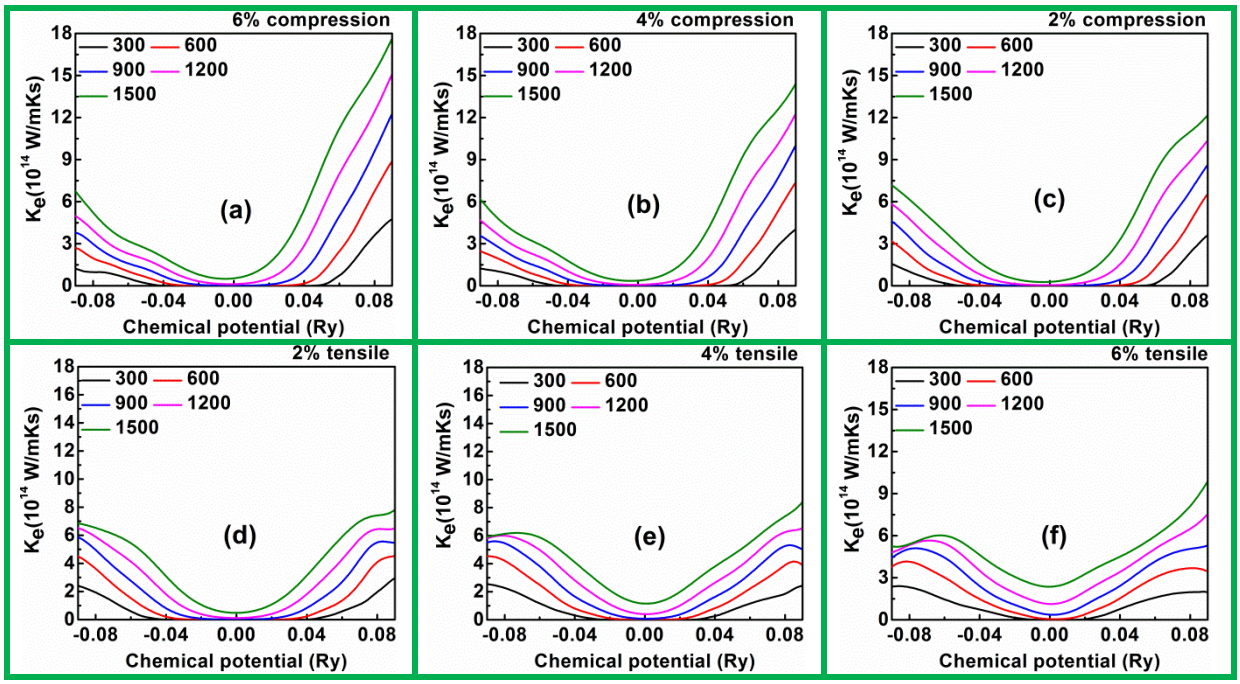

Figure 7.8 Chemical potentials dependent electronic thermal conductivity of WSSe monolayer at different temperatures for (a) – 6%, (b) - 4%, (c) -2%, (d) 2%, (e) 4% and (f) 6% strain (negative sign indiacates the compressive strain and postitive sign indicates the tensile strain)

Biaxial compressive and tensile strain dependent lattice thermal conductivity is calculated, shown in Figure 9(b). The lattice thermal conductivity decreases with increasing the tensile strain because of weakening the interatomic forces between the atoms (K. Yuan, Zhang, Li, & Tang, 2019). Moreover, the thermal conductivity increases with the compressive strain. The impact of strain on the thermal conductivity of the crystalline materials can be understood as $\sim \epsilon^{-\gamma}$, where γ is the material dependent parameter. The power law can be interpreted as mainly due to the effect of both phonon relaxation time and group velocity as $\tau \sim \epsilon^{-(2\alpha+2\beta)}$ and $v_g \sim \epsilon^{-\alpha}$; where

$\gamma = 4\alpha + 2\beta$ and both α and β are the material dependent parameters (Seijas-Bellido, Rurali, Íñiguez, Colombo, & Melis, 2019). The change in the lattice thermal conductivity can be explained using the phonon band dispersion relation as acoustic and optical phonon modes are both responsible for a change in the lattice thermal conductivity. The acoustic and optical modes get hardened under compressive strain, which increases the phonon group velocity, shown in Figure 7.9(a). Further, the frequency gap between optical and acoustic modes decreases significantly under the biaxial compressive and tensile strain suggesting the enhanced phonon-phonon interaction. The reduction rate of the frequency gap i.e. the ratio of frequency gap with applied strain is more in compressive strain with respect to the tensile strain, shown in Figure 7.9(a). The lower frequency i.e. acoustic modes are more responsible for thermal conductivity as compared to the higher frequency i.e. optical modes. The vibrational modes with frequency < 5.2 THz are the acoustic modes, which are dominated in lattice thermal conductivity. The softening of acoustic modes reduces the group velocity and increases the phonon scattering rate, causing a reduction in thermal conductivity. Moreover, the hardening of modes improves the group velocity; as a result, the lattice thermal conductivity improves. Lattice thermal conductivity is obtained by fitting $k_{lat}\ \alpha\ \frac{1}{T}$, which is valid for anharmonic phonon–phonon interaction (Seijas-Bellido et al., 2019). The computed lattice thermal conductivity under the biaxial strain is shown in Figure 7.9(b). The lattice thermal conductivity decreases by about 60% under the tensile strain (8%) as compared to the unstrained monolayer at room temperature (300K).

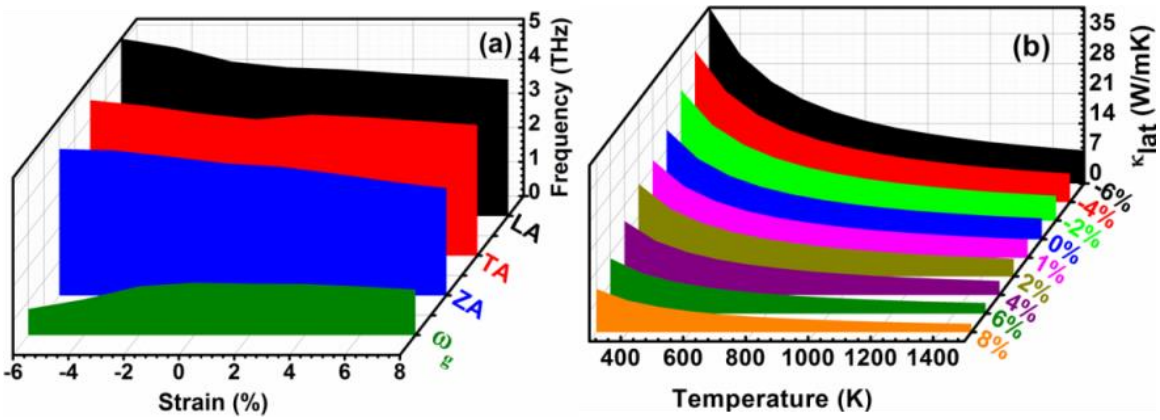

Figure 7.9 The variation in (a) frequency of LA, TA and ZA modes and group velocity against strain and (b) Lattice thermal conductivity against temperature at different strain values for WSSe monolayer.

After the calculation of the electrical conductivity and Seebeck coefficient, the relaxation time scaled power factor under the biaxial tensile and compressive strains are calculated at different temperatures are shown in Figure 7.10 for both n and p-type carriers. The peak of power factor increases with the chemical potentials (carrier concentration), and the maximum value for n-type carriers is 6.03×10^{11} W/mK²s noticed at 1500K under 2% compressive strain. In addition, the p-type carriers have highest value of power factor 3.14×10^{11} W/mK²s at 2% compression strain and 1500K. Here, we find that the compressive strain is more sensitive to improve the power factor compared to the tensile strain. The strain modulated power factor results suggest that n-type carriers in WSSe plays a significant role in achieving enhanced power factor under compressive strain. The power factor for n-type carriers is almost twice that of p-type carriers. The power factor is plotted in Figure 10 for different strains and noticed that it decreases for both strains with respect to the unstrained WSSe monolayer for both the carriers except 6% tensile strain. We also noticed that the value of band gap decreases on either side of 0% strain, and as a result of which the electrical conductivity, mainly for lower carrier concentration increases on either side of the unstrained case. The power factor is greater for n-type carriers under compressive strain and tensile strain and is attributed to the higher Seebeck coefficient contribution. The electronic conductivity at various temperatures is increase with increasing the compressive strain for n-type

carriers. In addition, the electrical conductivity is decreasing with increasing the tensile strain for n-type carriers. The maximum values of thermal conductivities for n(p)-type carriers at 1500K are 5.45(2.45)x10^{11}, 5.60(2.83)x10^{11}, 6.03(3.14)x10^{11}, 4.30(2.6)x10^{11}, 3.67(1.67)x10^{11} and 4.29(1.91)x10^{11} W/mK^{2}s for - 6%, - 4%, - 2%, 2%, 4% and 6% strain, respectively. The power factor for n-type carriers is almost double compare to p-type carriers. So we can ensure that n-type doping is more prominent for improving the power factor of WSSe monolayer.

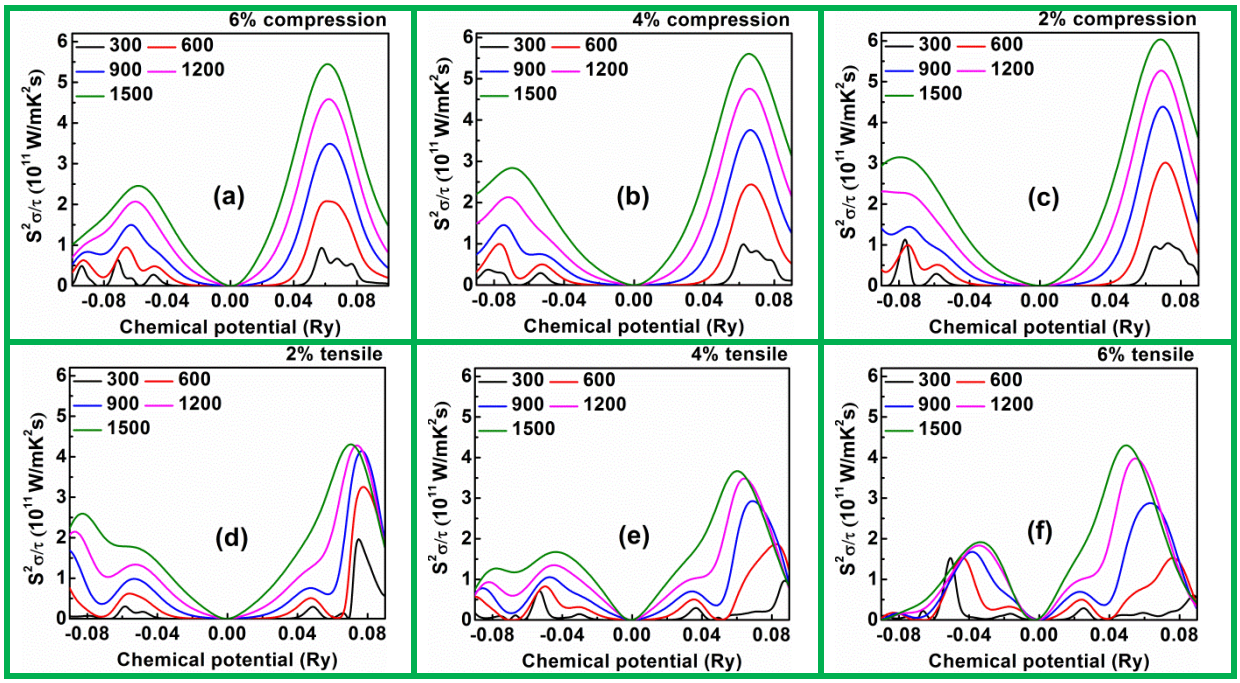

Figure 7.10 Chemical potentials dependent power factor of WSSe monolayer at different temperatures for (a) – 6%, (b) - 4%, (c) -2%, (d) 2%, (e) 4% and (f) 6% strain (negative sign indicates the compressive strain and postitive sign indicates the tensile strain)

The biaxial tensile and compressive strain dependent figure of merit is shown in Figure 7.11. The figure of merit for n-type carriers increases for tensile strain and decreases for compressive strain, while an opposite behavior is shown for p-type carriers. For n-type carriers, thermal conductivity dominates over power factor in case of tensile strain, and as a result, ZT increases with applied tensile strain. In the case of compressive strain, thermal conductivity seems to be dominated that's why the figure of merit of p-type carriers. In contrast for n-type carriers, ZT exhibits opposite characteristics and it decrease for compressive strain. The figure of merit at 1500K for n(p) carriers is 0.81(1.08), 0.89(1.07) and 0.99(0.87) at - 6%, - 4% and – 2% compressive strain, respectively. In contrast, figure of merit for at 6%, 4% and 2% tensile strain is 0.90(0.65), 0.99(0.62) and 1.25(0.72), respectively. The n-type carriers have significant impact to improve the figure of merit from 0.90 to 1.25 because lattice thermal conductivity is decline very sharply against the tensile strain. The maximum value of ZT is noticed at 1500 K and is around 1.25 and 1.08 for n and p-type carriers at 6% tensile and compressive strains, respectively.

Further, the figure of merit can be used to predict the efficiency of the thermoelectric device. Here, we considered a combination of n- and p- type WSSe monolayers, as shown in Figure 7.12 (a), to realize a thermoelectric device. The efficiency of the thermoelectric device can be predicted using the following relation (Snyder & Snyder, 2017):

$$\eta = \frac{T_H - T_C}{T_H} \frac{\sqrt{1+ZT}-1}{\sqrt{1+ZT}+{T_C}/{T_H}} = \eta_C \frac{\sqrt{1+ZT}-1}{\sqrt{1+ZT}+{T_C}/{T_H}}$$

Where T_C and T_H are cold and hot junction temperatures, respectively. Here, we have considered T_C ~ 300 K and varied T_H from 300 K to 1500 K, and maximum values of ZT are considered under

unstrained and strained WSSe monolayers with respective n and p-type doping. The thermoelectric efficiency for unstrained and strained monolayers are plotted in Figure 7.12(b) in the range of 300 K to 1500 K. The maximum efficiency for unstrained and strained devices is 17.7% and 22.6%, respectively. Thus, the strain mediated valley degeneracy and lattice thermal conductivity resulted in 28% enhancement in the thermoelectric efficiency with respect to unstrained monolayers.

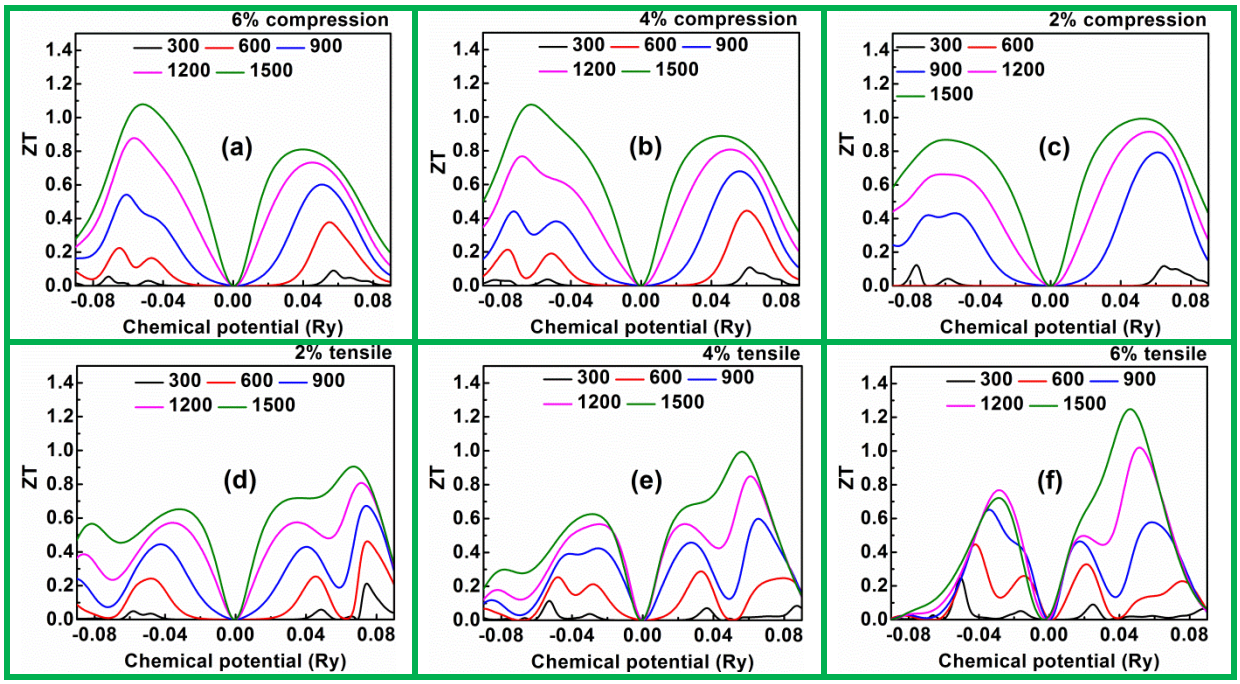

Figure 7.11 Chemical potentials dependent figure of merit of WSSe monolayer at different temperatures for (a) – 6%, (b) - 4%, (c) -2%, (d) 2%, (e) 4% and (f) 6% strain (negative sign indicates the compressive strain and postitive sign indicates the tensile strain)

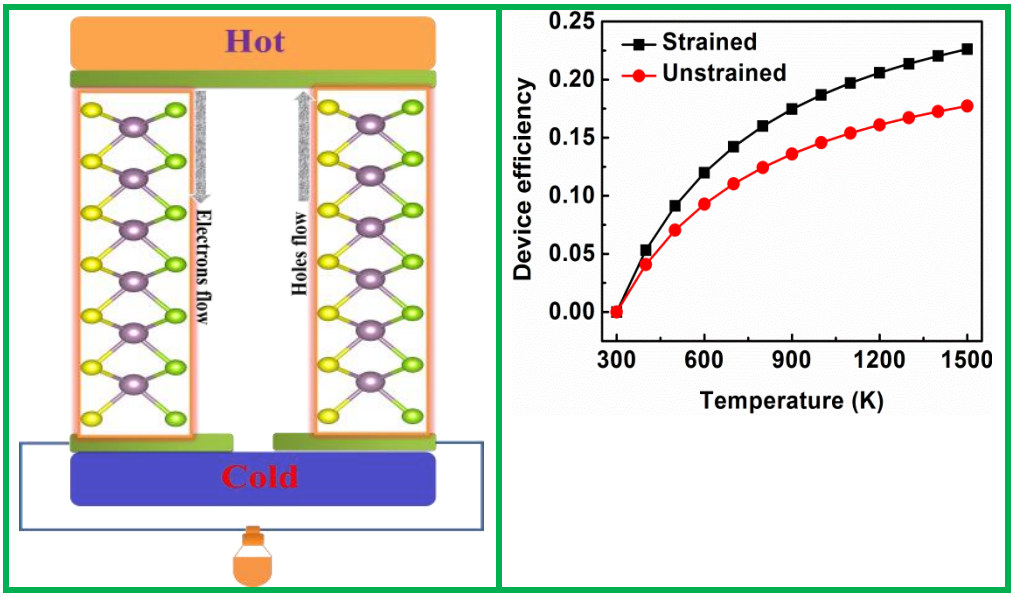

Figure 7.12 (a) Schematic representation of WSSe monolayer based thermoelectric device, and (b) the comparison of thermoelectric device efficiency against temperature for unstrained and strained WSSe monolayers

7.4 Conclusion:

We have systematically investigated the thermoelectric properties in terms of Seebeck coefficient, electrical conductivity, electrical thermal conductivity, lattice thermal conductivity, power factor, and figure of merit for unstrained Janus WSSe monolayer. The lattice thermal conductivity reduces with increasing the temperature. The thermoelectric response of the unstrained Janus WSSe monolayer is found more than of WS_2 and close to WSe_2 monolayers. The dynamic stability of biaxial strained monolayers is investigated using phonon dispersion, and is stable from 6% compressive strain to 8% tensile strain. Electrical conductivity and Seebeck coefficient are enhanced under biaxial strain due to valley degeneracy in the valence and conduction band edges. The lattice thermal conductivity is increasing under the compressive strain, which decreases under the tensile strain. The figure of merit due to biaxial strain improved from 0.90 (0.74) to 1.25 (1.08) for n(p)-type carriers. The thermoelectric device efficiency has increased by 28% for strained WSSe monolayer with respect to the unstrained WSSe monolayer. These results suggest the strain modulated valley degeneracy may provide a way to realize the enhanced thermodynamic efficiency of nano thermoelectric devices.